

PACS numbers: 42.79.Pw; 42.30.-d; 42.15.Dp
DOI: 10.1070/QE2005v035n01ABEH002897

A phase-knife wave-front sensor

A.S. Goncharov, A.V. Larichev

***Abstract*. The use of an optical system with a phase knife is proposed to record qualitatively the shape of the optical-radiation wave front. Theoretical and numerical studies of a sensor based on a phase knife are performed, the algorithms for reconstruction of the phase function and schemes for sensor realisation are developed, and the range in which the device can be used expediently is determined. The sensor component parameters required for its realisation are determined, and the sensor efficiency in various operational modes is tested experimentally.**

Keywords: *aberration, phase knife, wave front, spatial spectrum, Fourier optics, phase function visualisation, adaptive optics.*

1. Introduction

Measurement of the phase profile of a light wave is essential for the solution of many research and applied problems in optical metrology [1], adaptive optics [2], laser physics [3], and ophthalmology [4], etc. All techniques of phase measurements in optics are based on a transformation of the initial light field resulting in the dependence of the intensity of the light beam incident on a photodetector on the required phase function [1]. A variety of techniques developed in recent years have made it possible to qualitatively estimate and measure the wave-front profile. The most popular among these are interference devices using a coherent wave summation [1] and Shack – Hartmann sensors in which the local tilt of a wave front is transformed into displacement of light spots at the focus of the lens raster [5]. Despite many advantages of these techniques, the range of their application is restricted due to a number of drawbacks. Thus, interferometers are highly sensitive to vibrations and require the coherent reference wave to be undistorted (except for the shearing interferometers) [6]); moreover, the procedure for processing of interference patterns is quite complicated [7] and is hard to realise in real time. The dynamic range and spatial resolution of the Shack – Hartmann sensor are connected rigidly with the lens raster parameters and cannot be changed during measurements.

A.S. Goncharov, A.V. Larichev Department of Physics, M.V. Lomonosov Moscow State University, Vorob'evy gory, 119992 Moscow, Russia; e-mail: larichev@optics.ru, goncharov@bk.ru

Received 1 October 2004; revision received 25 November 2004
Kvantovaya Elektronika **35** (1) 91 – 96 (2005)
Translated by Ram Wadhwa

The accuracy of measurements in both these methods deteriorates considerably in the case of the amplitude modulation of the light wave. The drawbacks of the conventional methods necessitate a quest for alternative approaches for solving the problem of wave-front profile measurement.

In recent years, significant progress has been made in the development of sensors of the wave-front curvature [8], the shadow instruments using beamsplitter pyramids [9], and modulation-spectral methods of phase reconstruction [10]. The curvature sensors are based on the local intensity modulation arising during detection of radiation with a curved wave front outside the pupil plane. This variation is associated with the local curvature of the wave front, i.e., depends in fact on the second spatial derivative. Therefore, the reconstruction of the wave-front profile requires the solution of the Laplace differential equation (the so-called transport equation) with appropriate boundary conditions, which are not known, as a rule. In actual practice, two intensity distributions corresponding to the planes in front of the pupil plane and behind it are recorded. This makes it possible to perform normalisation for reducing the effect of the amplitude modulation [8].

A sensor with a pyramidal beamsplitter [10] is an interesting development of the Foucault shadow technique [11]. In this sensor, the distribution of light in the focal plane is split by a tetrahedral pyramid into four quadrants in which the emitted radiation propagates at a small angle to the optical axis and forms four images of the pupil in the plane of the phototdetector. Each of these images is similar to the pattern obtained from the Foucault knife placed on the left, right, top and bottom of the optical axis. The intensity distribution in the Foucault pattern is proportional (in the first approximation) to the spatial derivative of the wave front, and hence the procedure of reconstructing the wave-front profile is analogous to the one used for the Shack – Hartmann sensor. The presence of four images makes it possible to normalise them and to reduce considerably the adverse effect of the amplitude modulation of the intensity.

Note that the effect of the amplitude modulation in all the above techniques can be diminished only through normalisation, and the efficiency of this procedure is limited by the signal-to-noise ratio of the photodetector and by the photonic noise. It should be interesting to develop a wave-front sensor in which the suppression of the amplitude modulation occurs along the optical path itself. Moreover, the problem of enhancing the sensitivity of the sensor during measurement of small deformations of the wave front is also quite important.

In this study, we propose to record the shape of the wave front by using a confocal four-focus system with a phase knife as a converter of the spatial spectrum of the signal.

A phase knife was used for visualising phase distortions long ago [12]; however, it was employed only for a qualitative evaluation of the phase distortion profile. In a modification of the phase-knife technique proposed recently [13], the linearity of the phase–intensity transformation was improved considerably and the first derivative of the phase function was visualised. It was shown that such a system is not very sensitive to the amplitude modulation of the input radiation [14]. However, this technique still remains only qualitative.

In this study, we propose and experimentally investigate a new technique for processing images obtained by using a phase knife. This technique yields quantitative results and hence makes it possible to measure the phase distribution of an optical wave.

2. Phase knife and processing of sensor signals

A classical phase knife is an optical element dividing the aperture of a light beam into two parts, the radiation in each part propagating a different optical path. The straight boundary between the two parts forms the edge of the knife. The parameters of the device are selected in such a way that the optical path difference between the light waves passing through the phase knife on either side of the edge is equal to half a wavelength. Such an optical element, placed at the focus of a confocal four-focus lens system, acts as a Fourier phase filter transforming the phase distribution into the intensity distribution.

Consider the functioning of this device by using the Fourier optics apparatus (see Fig. 1 below). We represent the light field at the input (plane A_1) in the complex form $A_{\text{in}}(x, y) = \rho(x, y)\exp(\text{i}\varphi(x, y))$, where $\rho(x, y)$ is the amplitude; $\varphi(x, y)$ is the phase of the input signal; x and y are the coordinates in the beam cross section.

It is well known that a lens forms at the focus a Fourier transform of the object placed at its front focus. Therefore, the signal in the knife plane (plane A_2) has the form

$$U_{\text{in}}(\xi, \eta) = \int A_{\text{in}}(x, y)\text{e}^{-(\text{i}\xi x + \text{i}\eta y)}\text{d}x\text{d}y = F\{A_{\text{in}}(x, y)\},$$

where the coordinates ξ and η, expressed in spatial frequency units, are connected with the real coordinates x and y through the relations $\xi = 2\pi x/\lambda f$ and $\eta = 2\pi y/\lambda f$; f is the focal length of the lens; and λ is the input signal wavelength. As mentioned above, the phase knife shifts the phase of a part of the spectrum relative to the other by π without changing the signal intensity. Therefore, the transfer function of an undisplaced knife can be written in the form $H(\xi, \eta) = \text{i}\,\text{sign}(\xi)$, while the complex amplitude after passage in the knife (plane A_3) can be represented as $U_{\text{out}}(\xi, \eta) = U_{\text{in}}(\xi, \eta)H(\xi, \eta)$. The second lens performs the inverse Fourier transform, forming the image

$$A_{\text{out}} = F^{-1}\{U_{\text{out}}(\xi, \eta)\} = F^{-1}\{U_{\text{in}}(\xi, \eta)\text{i}\,\text{sign}(\xi)\}$$

$$= A_{\text{in}}(x, y) \otimes (1/\pi x) = \frac{1}{\pi}\int \frac{A_{\text{in}}(x', y)}{x' - x}\text{d}x',$$

in the A_4 plane, where $1/\pi x = F\{\text{i}\,\text{sign}(\xi)\}$. Thus, we can write

$$A_{\text{out}}(x, y) = \aleph\{A_{\text{in}}(x, y)\}, \tag{1}$$

where $\aleph\{A_{\text{in}}(x, y)\}$ is the Hilbert transform equivalent to the operation of differentiation for narrow-band signals [10]. Hence, for a constant intensity, the amplitude at the output of the system will be proportional to the derivative of the phase function $\varphi(x, y)$. Because the detectors record the intensity of light, it is possible to measure only the square of the derivative in actual practice.

By displacing the edge of the phase knife in the transverse direction, we can make the system sensitive not only to the amplitude of phase inhomogeneities, but also to the sign of the local slope of the wave front. In this case, the zero-order spatial frequency will be no longer suppressed due to destructive interference, and the intensity of the output signal will be proportional to the derivative of the phase distribution.

Consider the operation of a displaced phase knife in the case of a harmonic phase modulation and an infinite aperture. By representing the phase distribution at the input to the system in the form $A_{\text{in}}(x) = \exp(\text{i}a_0\cos(vx))$, we can write

$$A_{\text{in}}(x) = J_0(a_0) + 2\text{i}J_1(a_0)\cos(vx) - 2J_2(a_0)\cos(2vx)$$

$$- 2\text{i}J_3(a_0)\cos(3vx) + \ldots,$$

where $J_j(a_0)$ is the Bessel function, $j = 0, 1, 2, \ldots$. Using formula (1) for the undisplaced knife and the properties of the Hilbert transform [11], we obtain

$$A_{\text{out}}(x) = \text{i}J_0(a_0) - 2\text{i}J_1(a_0)\sin(vx)$$

$$+2J_2(a_0)\sin(2vx) + 2\text{i}J_3(a_0)\sin(3vx) - \ldots,$$

where the zeroth harmonic is multiplied by i to take into account the displacement of the knife. By calculating the signal intensity from the expression $I_{\text{out}}(x, y) = |A_{\text{out}}(x, y)|^2$, we obtain

$$I_{\text{out}} = 1 - (4J_1J_0)\sin(vx) - (2J_1^2 + 4J_1J_3 + 2J_2J_4)\cos(2vx)$$

$$+ (4J_3J_0)\sin(3vx) + (4J_1J_3 - 2J_2^2)\cos(4vx) - \ldots. \tag{2}$$

For relatively low phase modulation depths, the coefficients of the appearing multiple frequencies are negligible, and the dependence of the output intensity on the derivative of the phase function is almost linear. However, as the modulation amplitude increases, nonlinear terms can no longer be neglected. To extend the range of the linear operation of the sensor, we will use the following procedure. We record the intensity distributions obtained by displacing the knife on either side of the zeroth diffraction order by the same value along both axes. Then, we calculate the normalised difference signal with the help of the relations

$$I_x(x, y) = \frac{I_{+\Delta x}(x, y) - I_{-\Delta x}(x, y)}{I_{+\Delta x}(x, y) + I_{-\Delta x}(x, y)},$$

$$I_y(x, y) = \frac{I_{+\Delta y}(x, y) - I_{-\Delta y}(x, y)}{I_{+\Delta y}(x, y) + I_{-\Delta y}(x, y)}. \tag{3}$$

Here the subscripts $\pm\Delta x$ and $\pm\Delta y$ denote the intensity distributions obtained upon a displacement of the knife. It can be easily verified that this procedure allows us not only to reduce the effect of amplitude fluctuations due to normalising to the total intensity, but also to reduce the influence of the nonlinearity due to the removal of even harmonics. The quantities $I_x(x, y)$ and $I_y(x, y)$ are proportional to the local slopes $d\varphi/dx$ and $d\varphi/dy$ of the wave front, respectively. Then, the phase distribution is reconstructed from the measured local slopes by the method of least squares [15]. Note that, unlike the widely used Shack – Hartmann wave-front sensors, the spatial resolution of the device is limited only by the number of elements in the photodetector.

3. Experimental realisation of the sensor

Figure 1 shows the experimental setup for studying the operation of the sensor. The setup is based on a confocal telescopic system working on the autocollimation principle. The source of radiation was semiconductor laser (*4*) coupled with a single-mode fibre. Laser radiation was coupled to the telescopic system using beamsplitter cube (*3*). This radiation was collimated by objective (*2*). A bimorphic deformable mirror fabricated at the adaptive optics laboratory of the Department of Physics, Moscow State University was located in the focal plane of objective (*2*). The construction of the mirror was similar to that described in [16] and made it possible to reproduce aberrations up to the fourth-order. The mirror was controlled by controller (*10*) connected to PC (*11*). The radiation reflected from the mirror passed through lens (*2*) and beamsplitter cube (*3*) in the opposite direction and was incident on phase knife (*5*) (a glass plate with a step profile). The plate was mounted on a micrometer translator which provided the necessary displacements in the plane perpendicular to the optical axis of the system. The radiation was then collimated by lens (*6*) to produce the beam of diameter of 3 mm required for matching the adaptive mirror aperture with CCD camera (*9*). The 6.8×4.8-mm CCD array containing 720×570 pixels was placed at the focal plane of lens (*6*) where the reduced image of the adaptive mirror was formed. The output signal from the camera was fed to the PC and was digitised by a Matpox MC frame-grabber with an 8-bit precision. Beamsplitter cube (*7*), which directs a part of the radiation to Shack – Hartmann sensor (*8*) consisting of a lens raster with a step of 0.2 mm and a focal length of 5.2 mm and a CCD array analogous to array (*9*), was placed between lens (*6*) and CCD camera (*9*). The Hartmann diagram was digitised with an 8-bit precision using the same PC. The sensor software made it possible to reconstruct the wave-front profile in the form of an expansion in 36 Zernicke polynomials. The mean square error of measurements was less than 0.04 μm.

4. Operation of a sensor with a point reference source

The operation of a sensor with a point reference source was studied both experimentally and numerically. The signals from the sensor were processed by using the central part of aperture comprising 0.8 of the overall beam aperture in order to eliminate the edge effects. A mesh with square cells was formed in this region. The intensity at the mesh nodes was calculated by averaging the intensity over a quadratic region with its centre at a mesh node and a side equal to the pitch of the mesh. A 20×20 mesh was used in the experiments.

Numerical simulation was performed in the parabolic approximation of the diffraction theory using the Fourier transform. It was assumed in calculations that the mesh consists of 512×512 elements, which is close to resolution of the CCD array used in the experiments. The sensor noise was simulated by adding uncorrelated noise with a Gaussian distribution to the computed values of the intensity at the sensor output. The noise dispersion corresponded to the Poisson statistics of photocounts and a potential well depth of 40000 photoelectrons. The obtained pattern was then processed by the same method as the pattern from the CCD sensor in the experiment.

Phase distortions were simulated by applying different voltages to the mirror electrodes. The resulting phase profile was controlled with the help of a Shack – Hartmann sensor, which was preliminary calibrated by means of a precision angular deflector and a reference mirror of high optical quality.

Figure 2 shows an example of the reconstruction of the aberrations pattern by a sensor with a phase knife. The figure also shows the results of numerical simulation, the input phase distribution corresponding to the Zernicke coefficients measured by a Shack – Hartmann sensor. One can easily see that the reconstructed and calculated patterns are almost identical, which points to the correctness of the sensor model. The slight discrepancy is due to the fact that the intrinsic aberrations of lens (*6*) almost do not affect the

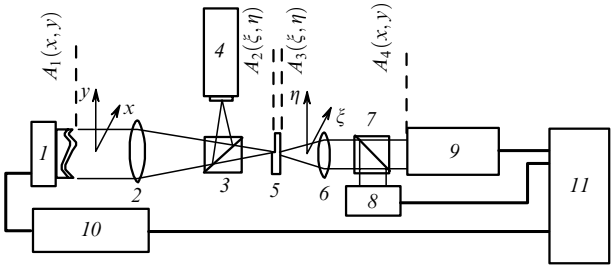

Figure 1. Scheme of a wave-front sensor based on a phase knife: (*1*) adaptive mirror; (*2*, *6*) lenses; (*3*, *7*) beamsplitter cubes; (*4*) laser; (*5*) phase knife; (*8*) Shack – Hartmann sensor; (*9*) CCD camera; (*10*) mirror controller; (*11*) PC.

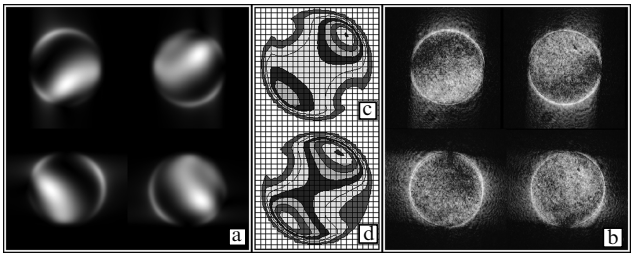

Figure 2. Output images obtained from a sensor by numerical simulation (a) and experimentally (b), and the reconstructed wave front obtained by simulation (c) and experimentally (d).

signal from the sensor with a phase knife (the knife is installed before the lens), while the Shack–Hartmann sensor measures total aberrations taking this lens into account.

The dependence shown in Fig. 3 also illustrates a good coincidence between the simulated and experimentally obtained values of the transfer function of the sensor. The transfer function was obtained for the aberrations (astigmatism), the controlling voltage at the mirror was changed smoothly in the experiment, while the amplitude of the initial phase modulation was measured by a Shack–Hartmann sensor. One can see that noticeable differences in the transfer functions appear for a phase modulation equal to about 1.5 wavelengths, which narrows the dynamic range of the sensor by about 25 %. However, the linearity of the transfer parameter is preserved in the operating range.

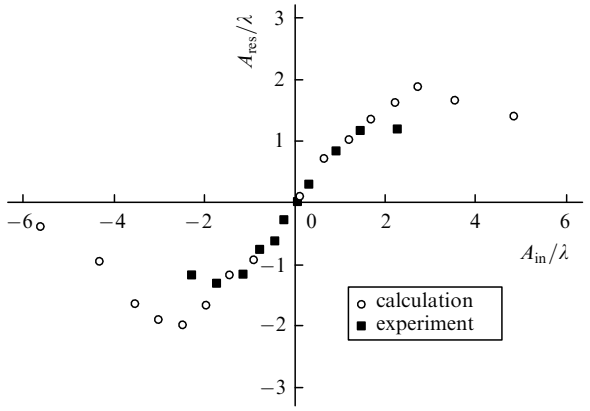

Figure 3. Dependences of the amplitude of the reconstructed phase function A_{res} on the initial function A_{in} represented by the second Zernicke polynomial (astigmatism); λ is the radiation wavelength.

Consider the effect of the amplitude modulation on the sensor operation. The amplitude modulation in the experiment was produced by a tie test pattern placed near the edge of beamsplitter cube (*3*) facing the laser. The test pattern had a 100 % transmission modulation. During numerical simulation, the amplitude modulation was produced at the sensor input (in the A_1 plane, see Fig. 1). Figures 4c and d show the result of the reconstruction of the phase profile in the presence of the amplitude modulation. Figure 4a shows the intensity distribution in the adaptive mirror plane where the intensity modulation is slightly lower than 100 % due to diffraction effects. One can see from Fig. 4 that the intensity modulation does not produce any noticeable distortions in the reconstructed phase profile.

Because a smooth variation of the amplitude modulation was difficult to produce in the experiment, the sensor parameters for various values of amplitude modulation were determined numerically. Figure 5a shows the modulation transfer curve for a sensor with a phase knife. For comparison, the same figure also shows the modulation transfer curve for a Foucault knife. Both dependences were obtained without using (3) for normalising the intensity. One can clearly see that the 50 % amplitude modulation is suppressed almost completely for the phase knife, while this does not occur for the Foucault knife.

To estimate the effect of the amplitude modulation on the accuracy of phase-profile measurements, we perform a

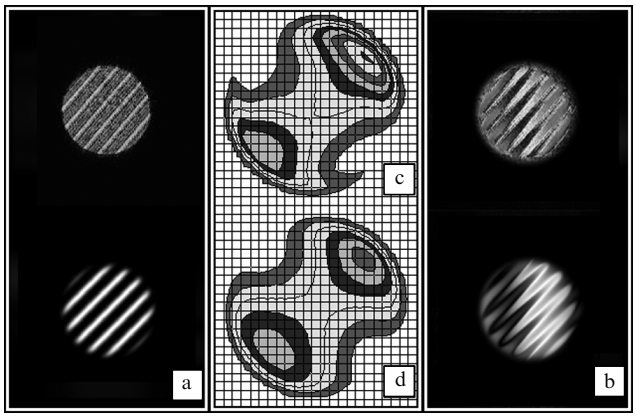

Figure 4. Intensity in the beam cross section (a), images obtained at the sensor output (b), and the wave front reconstructed in the experiment (c) and in the computer model of the sensor (d) for the sensor operating with a beam with the 100 % intensity modulation in its cross section.

numerical experiment in which the amplitude modulation is described by a random combination of 36 Zernicke polynomials (Fig. 5b). Because the phase distortions were also specified in the form of Zernicke polynomials (in our experiment, it was a coma with an amplitude of 2.5 rad), such a case was the most unfavourable for the sensor operation. Ten trials were performed for each value of the modulation, and the results were averaged. One can see that the error was quite low even for large intensity fluctuations, which is a merit of the normalisation algorithm (3). Note that the reconstruction error increases considerably for the Foucault knife at high levels of the amplitude modulation, while such an increase for a phase knife is insignificant. Such a behaviour could be anticipated in view of the form of the amplitude modulation curves.

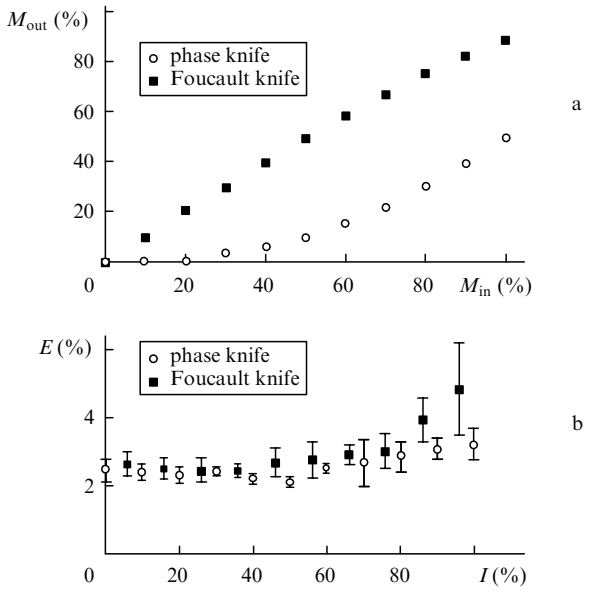

Figure 5. (a) Dependences of the amplitude modulation M_{out} at the system output on its modulation M_{in} at the input and (b) the dependence of the wave front reconstruction error E (per cent of the input phase modulation amplitude) on the modulation amplitude of the input signal intensity I.

Even for the 100 % amplitude modulation at the input in the case of a phase knife, the modulation at the output does not exceed 50 %, but this does not deteriorate the efficiency of the normalisation procedure.

5. Operation of a sensor with a distributed source

So far, we have considered a case in which the source image at the phase knife in the absence of phase distortions is limited by diffraction (i.e., has the form of an Airy disc, whose angular dimensions are determined by the diameter of the input aperture). In most cases of practical importance, however, the radiation source is not point like and spatially coherent, i.e., its image in the knife plane is much larger than the Airy disc (see Fig. 1). Recall that the phase knife visualises only those spatial frequencies whose spectral components lie on both sides of the knife. For a spatially incoherent source, each point of the source (i.e., each coherent region) is processed independently by the phase knife, and the obtained signals are then accumulated incoherently on a photodetector.

Phase distortions with an angular size smaller than the angular size of the source are well visualised for all points of the source, while phase distortions of a large angular size are visualised only in a small region of the source. The rest of the source produces only a uniform background. Therefore, if the source has a uniform brightness and size in a direction parallel to the edge of the knife, the amplitude of visualised distortions increases linearly with the spatial frequency. This effect produces a frequency multiplier in front of the Hilbert transform [see Eqn (1)] required for obtaining an exact derivative. It can be expected that the range of linear response of the sensor will increase for a distributed source, and the dependence will be preserved over a broader spectrum of phase distortions for larger angular dimensions of the source.

In actual practice, the angular size of the source is limited by the isoplanatic region of the given phase distortions. In addition, an increase in background illumination will hamper image recording at the output of the sensor (reduce the signal-to-noise ratio).

A 650-nm LED was used instead of a semiconductor laser in the experiments for creating a distributed source. The plastic lens of the diode was removed and the endface of the casing was polished to optical quality. The light-emitting area of the diode was a square of size about 1.5 mm corresponding to an angular size of 30″. Figure 6 shows the dependence of the amplitude of the reconstructed phase on the amplitude of the phase modulation at the sensor input. The parameters of the experiment are the same as for the amplitude modulation. One can clearly see that the range of linear operation of the sensor in the experiment with a distributed source is more than five times broader than this range in the experiment with a point source.

It can be assumed that there exists an optimal angular size of the source for certain orders of aberrations, because an increase in the source size reduces the signal-to-noise ratio, but at the same time the linear dependence of the visualised derivative of the spatial frequency is violated for small sizes of the source. Figure 7 shows the numerically determined dependences of the mean square error in reconstruction for various orders of aberrations on the angular dimension of the source. One can clearly see

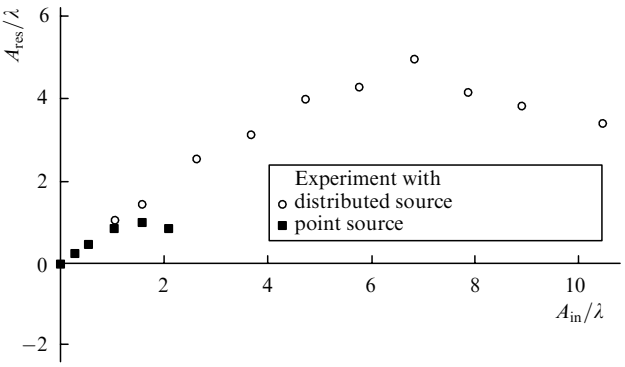

Figure 6. Dependences of the amplitude A_{res} of the reconstructed phase function on the initial function A_{in} defined by the second Zernicke polynomial (astigmatism); λ is the radiation wavelength.

that for low (third and fifth) orders of aberrations, the optimal source size should be quite small (about 20″), while a well-defined minimum exists for an angular source size of 100″ in the case of higher (seventh-order Zernicke polynomials) order aberrations. This means that the optimal source size in actual practice must be chosen in accordance with the spatial parameters of the aberrations being measured. If it is not possible to vary the source size, e.g., in problems of remote sensing, specially designed phase screens [17] can be used for obtaining the required distribution at the phase knife.

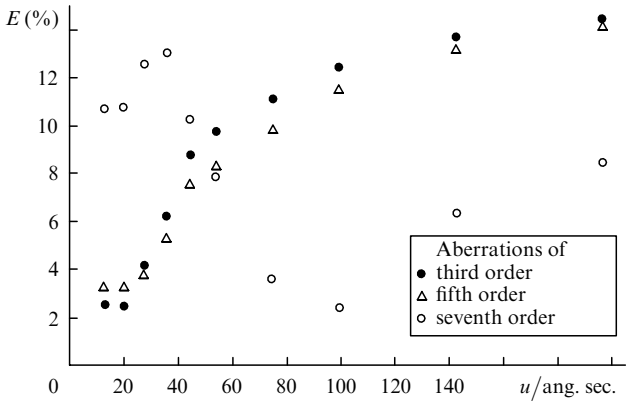

Figure 7. Dependences of the wave-front-reconstruction error E (per cent of the input phase modulation amplitude) on the angular size of the distributed reference source taking into account the third-, fifth- and seventh-order aberrations.

6. Conclusions

An analysis of the obtained data has shown that the wave-front sensor with a phase knife has several advantages over the conventional methods of phase measurement. First of all, this is a low sensitivity to the spatial amplitude modulation of the radiation under investigation. The advantages of the sensor are especially obvious when the procedure of intensity normalisation is inefficient, i.e., in the regime of low intensities when the photon noise of the photodetector is high, and in regimes with a high amplitude modulation. The sensitivity of the device proposed in the

paper is twice as high as that of a wave-front sensor with a Foucault knife [10]. Therefore, the sensor with a phase knife is preferable for measuring small phase distortions.

Naturally, a practical realisation of the device does not require a mechanical displacement of the phase knife in the focal plane as was done in the experiment. It is more reasonable to form four multiplication patterns of the source using diffraction gratings. In this case, all the four images of the pupil can be formed simultaneously on a single CCD sensor, as in the case of a sensor with a beamsplitter pyramid [10].

A disadvantage of the sensor is its rather complicated design. However, the required optical elements can be prepared quite economically using modern technologies of photolithography and plastic replication.

Acknowledgements. The authors thank V.I. Shmalgauzen for useful advice and comments, and N.G. Iroshnikov for his help in the software development. This work was supported by the Russian Foundation for Basic Research (Grant No. 04-02-16876-a).

References

1. Malakara D. (Ed.) *Opticheskii proizvodstvenniy kontrol* (Optical Production Control) (Moscow: Mashinostroenie, 1985).
2. Vorontsov M.A., Koryabin A.V., Shmalgauzen V.I. *Upravlyaemye opticheskie sistemy* (Controlled Optical Systems) (Moscow: Nauka, 1988).
3. Baumhacker H., Pretzeler G., Witte K.J., Hegelich M., Kaluza M., Karsch S., Kudryashov A., Samarkin V., Rukosuev A. *Opt. Lett.*, **27** (17), 1570 (2002).
4. Liang J., Grimm B., Goelz S., Bille J.F. *J. Opt. Soc. Am. A,* **11**, 1949 (1994).
5. Platt B., Shack R.V. *Opt. Sci. Center News*, **5** (1), 15 (1971).
6. Shekhtman V.N., Rodionov A.Yu., Pel'menev A.G. *Opt. Spektr.*, **79** (1), 134 (1995).
7. Malacara D., Servin M., Malacara Z. *Interferogram Analysis for Optical Testing* (New York: Marcel Dekker, 1998).
8. Blanchard Paul M., Fisher David J., Woods Simon C., Greenaway Alan H. *Appl. Opt.*, **39** (35), 6649 (2000).
9. Ragazzoni R. *J. Mod. Opt.*, **43**, 189 (1996).
10. Zelepukina E.V., Zubov V.A., Merkin A.A., Mironova T.V. *Opt. Spektr.*, **93** (5), 814 (2002).
11. Soroko L.M. *Gil'bert-optika* (Hilbert Optics) (Moscow: Nauka, 1981).
12. Lowenthal S., Belvaux Y. *Appl. Phys. Lett.*, **11** (2), 49 (1967).
13. Larichev A.V., Nikolaev I.P., Costamagna S., Violino P. *Opt. Commun.*, **121**, 95 (1995).
14. Nesteruk K.S., Nikolaev I.P., Larichev A.V. *Opt. Spektr.*, **91** (2), 320 (2001).
15. Southwell W.H. *J. Opt. Soc. Am. A*, **70**, 998 (1980).
16. Dainty J.C., Koryabin A.V., Kudryashov A.V. *Appl. Opt.*, **37**, 4663 (1998).
17. Ragazzoni R., Diolaiti E., Vernet E. *Opt. Commun.*, **208**, 51 (2002).